SUPPORTING TEXT

1. Surface-Initiated Assembly: Fibronectin NanoFabrics as a Paradigm for Engineering the Extracellular Matrix

1.1. Fibronectin fibrillogenesis in vivo and in vitro

For protein fibrillogenesis to occur, intermolecular binding domains within the individual molecules must interact under specific conditions to form protein fibrils. We focus on FN because in wound healing and development the initial ECM is often a FN matrix,[1] which then serves as a template for subsequent collagen fibrillogenesis. The assembly of FN dimers into fibrils requires force to unfold the molecule and expose cryptic FN-FN binding domains.[2] Cells *in vivo* use integrin receptors to bind FN dimers and apply force to mediate assembly.[2, 3] Cells *in vitro* use the same integrin-mediated process, either secreting FN themselves or using the FN present in serum. However, it has proven difficult to recapitulate this force-based FN nano-assembly without cells.

Recent work has demonstrated initiation of FN fibrillogenesis *in vitro* and in a cell-free system by applying force to FN solutions at interfaces. Microscale FN fibrils can be drawn from FN droplets[4] and nanoscale FN fibrils can created by de-wetting FN solutions from microengineered surfaces.[5] Related, tubular FN mats will form from solution on the shafts of high-speed motors due to shear force.[6] These examples demonstrate the concept of using interfacial energy to drive fibrillogenesis, but are limited to specific geometries and/or are bound to surfaces. The question is whether this cell-free approach can be expanded beyond FN to create a robust system to engineer ECM proteins into complex, multi-component matrices.

1.2. Unfolding of fibronectin at surfaces

We reasoned that protein-surface interactions (surface energy) could be used to unfold ECM proteins like FN in lieu of surface tension[4, 5] or shear force.[6] Research on blood-contacting surfaces has established that FN and other serum proteins denature (unfold) onto polymeric surfaces.[7] This process is driven by polar and non-polar interactions between amino acids in the protein backbone and chemical moieties at the material surface. AFM has shown that FN dimers adsorbed onto hydrophobic and hydrophilic surfaces unfold from the globular, solution conformation into an extended, rod-like conformation.[8-10] We can infer how the FN unfolds on the surface from the molecular structure. The disulfide-bonded FN homodimer consists of three main type I, II and III repeat motifs[11, 12] that contain β-sheet secondary structure, but the type I and II repeats are stabilized by interior disulfide-bridges. Thus, FN unfolds on surfaces via loss of tertiary structure from the solution conformation and potentially loss of secondary structure of the type III repeats. FRET studies sensitive to type III repeat structure have confirmed that both surface interactions[13, 14] and physiologic forces[15, 16] are able to unfold these domains. Fibrillogenesis can potentially occur when this surface induced unfolding exposes cryptic FN-FN binding domains and the unfolded dimers are close enough to interact.

1.3. Fibronectin fibrillogenesis at surfaces

Studies have shown that FN fibrillogenesis occurs by binding of the first five type I repeats and the second type III repeat.[2, 11, 17, 18] Fluorescently labeled 70 kDa N-terminal FN fragments (containing the first five type I repeats) bind to assembling fibrils in cell culture[12] and pulled fibrils,[4] which suggests cryptic FN-FN binding domains are exposed during cell-mediated and cell-free fibrillogenesis. We propose that the same process occurs during surface-initiated assembly (Fig. 1). The fibrillar morphology reported for FN adsorbed to surfaces[8] is comparable to that observed in FN nanoFabrics (Fig. 4a-c), structurally verifying the FN has unfolded. Normally this adsorption of FN and other proteins to surfaces is an irreversible process as the unfolded molecules are ‘pinned-down’ by surface

energy. Thus, for surface-initiated assembly, the real challenge is fibril formation and non-destructive release, which requires altering surface properties on command to 'un-pin' the FN.

Surface-initiated assembly on poly(N-isopropylacrylamide) (PIPAAm) achieves this goal by creating free-standing, nanoFabrics from FN and other ECM proteins. In this process, ECM proteins are initially adsorbed to a relatively hydrophobic polydimethylsiloxane (PDMS) substrate to unfold the protein (Fig. 1).[19-23] The FN is then transferred in this unfolded state from the PDMS onto a relatively hydrophilic PIPAAm surface by conformal contact. It is not known whether assembly occurs in a dry state on the PDMS or PIPAAm, in a hydrated state on PIPAAm at >35ºC or if it occurs as the PIPAAm becomes more hydrophilic and dissolves during the thermal transition. However, assembly has clearly occurred, because as the PIPAAm dissolves protein nanoFabrics are released as an insoluble matrix with the topology defined by the patterning (Fig. 3a and 3b). The FN nanoFabrics were coupled together via specific hydrogen binding, as they supported >15-fold extensibility while remaining in fibril form. However, we know this was non-covalent binding as the FN nanoFabrics dissolved in a 1% sodium dodecyl sulfate solution, suggesting that the fibrils were stabilized by hydrogen bonding, comparable to nascent cell-assembled FN matrix.[11]

Protein nanoFabrics are released using a non-cross-linked PIPAAm that completely dissolves—a technique different from the engineered cell sheets pioneered by Okano and coworkers.[24-27] This complete dissolution is the only way to non-destructively release a protein nanoFabric <10 nm thick from the PIPAAm surface. Okano and co-workers, however, used cross-linked PIPAAm grafted to Petri dishes, which does not dissolve thus leaving a nanometer thick layer of ECM proteins entrapped in the PIPAAm.[28] This works for their purpose because the cell-sheet technique relies on the adhered cells to mediate assembly of FN and other ECM proteins into a matrix.[27] They have used this to create isotropic cell sheets, but only one recent example has shown the ability to create aligned cell sheets.[29] The advantage of our protein nanoFabrics is that the patterned matrix is released with the cells, enabling the continued alignment of cells post release (Fig. S3a). Furthermore, protein nanoFabrics enable us to dictate the exact protein composition and hierarchical structure of the matrix to serve as a template for subsequent cell attachment and growth, rather than relying purely on a cell-generated matrix with minimal control of composition or fidelity. We have not detected any trace amounts of PIPAAm in the protein nanoFabrics during our optical and mechanical analysis or cell assays, nor do the nanoFabrics expand/contract during thermal cycling through the LCST. Thus, any potential PIPAAm trapped in the nanoFabrics is below the detection limit, and since it is polymerized, is not toxic to cells even if it is present.[30]

2. Stretching NanoFabrics with Cardiomyocytes: A Cell-Based Assay

Cardiomyocytes were used in this study to determine whether the integrin-binding domains in FN-III_{10} were functional and whether the nanoFabrics could support cell-generated forces. As an extreme test, we demonstrated that single, 20 µm wide, millimeter-long FN nanoFabric strands suspended in media were able to bind passively seeded cardiomyocytes, support cell-cell coupling into a myocardial tissue and withstand the cyclic force generated by contractions. This confirmed that -RGD- integrin binding sites were accessible at a physiologically relevant density to bind cardiomyocytes. It is unlikely that cardiomyocytes crawled onto the FN nanoFabric from the surrounding PDMS frame because they are non-migratory cells. Synchronous contraction of the cardiomyocytes (Fig. 6e and Supplementary Information, Movie S8) indicated that the cells were able to elongate along the FN nanoFabric and couple to one another to form a continuous, myocardial tissue strand. We previously estimated the force generated by aligned cardiomyocytes as a specific force of ~4 mN/mm^2.[21] Thus, the nanoFabrics appear to support a similar force regime over a multiday time course.

The folding/unfolding of FN type III repeats suggested by the SEM and AFM analysis (Fig. 4 and 5) likely underlies this extensibility. Unfolding of globular protein domains is a common structural motif

to store mechanical energy in biological systems.[31] The sarcomeric protein titin contains a series of β-sheet rich domains (I91, formerly I27) that unfold/refold providing passive elasticity to striated muscle. Similar domains exist in FN matrix, specifically the type III repeats (FN-III) that have comparable unfolding forces (~100 pN) and contour lengths (~30 nm).[32, 33] Interestingly, the FN-III has partially unfolded intermediates[31, 33] that impart additional mechano-functionality, including cryptic anastellin within FN-III_1 that has anti-metastatic properties. This suggests an interesting possibility, that FN nanoFabrics may have tunable biological and pharmacological properties controlled by mechanical strain.

EXPERIMENTAL METHODS

1. Protein nanoFabric fabrication

Glass cover slips (25 mm diameter) were coated with poly(N-Isopropylacrylamide) (PIPAAm) by spin coating on a 10% PIPAAm (Polysciences, Inc.) in 1-butanol (w/v) solution. The 1-butanol evaporated during spin coating leaving a ~1 μm thick layer of PIPAAm. The PIPAAm coated cover slips were subsequently sterilized using high-intensity UV light for 8 minutes. Extracellular-matrix (ECM) proteins were patterned onto the PIPAAm coated cover slips by microcontact printing (μCP) using polydimethylsiloxane (PDMS, Sylgard 184, Dow-Corning) stamps. The basic μCP technique is well established and allows the rapid patterning of biomolecules on a variety of planar substrates using PDMS stamps.[19, 34] PDMS stamps were fabricated [based on established methods][21] with various geometries including; (i) 20 μm wide, 20 μm spaced, 2 μm tall ridges (20x20); (ii) 15 μm wide, 15 μm spaced, 2 μm tall ridges (15x15); (iii) 10 μm wide, 10 μm spaced, 2 μm tall ridges (10x10); and (iv) net-like patterns with 10x30 μm elliptical pores or 15x20 μm elliptical pores, hexagonally packed. Briefly, silicon wafers were spin coated with SU-8 photoresist (Microchem) and exposed to UV light through a photomask, selectively cross-linking regions of the photoresist. The photoresist was then developed and the non-exposed regions were removed. A negative of the patterned photoresist wafer was formed by casting PDMS prepolymer against it. Prior to each use, the PDMS stamps were sonicated in 50% ethanol for 30 minutes to sterilize and remove surface contaminants. Once dried, the PDMS stamps were inked with a 250 μL droplet of ECM protein in DI water and incubated for 1 hour. The ECM proteins used to ink the PDMS stamps for this study were FN from human plasma at 1, 2.5, 5, 10, 25, 50 and 100 μg/mL,[35] LAM and COL_{IV} from Engelbreth-Holm-Swarm murine sarcoma basement membrane at 50 μg/mL and 200 μg/mL respectively, COL_I from rat tail at 1 mg/mL, COL_I-FITC conjugate from bovine skin at 1 mg/mL, and FIB from bovine plasma at 50 μg/mL (Sigma-Aldrich). The concentrations used for LAM, COL_I, COL_{IV}, FIB and FN at 1 μg/mL represent the minimum for which protein nanoFabrics were consistently generated. The PDMS stamps were subsequently rinsed twice in DI water to remove excess protein and dried under a stream of compressed air. ECM proteins were then transferred to the PIPAAm surface using single or multiple stampings, depending on the specific nanoFabric being fabricated. For each stamping, the PDMS stamp was placed in conformal contact with the PIPAAm for 5 minutes; longer contact times did not increase protein transfer. The protein nanoFabrics were released from the PIPAAm by taking advantage of the thermal transition of PIPAAm at its lower critical solution temperature (~35ºC). Dissolution of the PIPAAm was achieved by either placing the cover slip in water below ~35ºC, or, if the cover slip was already placed in heated water (>35ºC), cooling below this temperature.

2. Analysis of protein nanoFabric patterning and release

The protein nanoFabrics (FN, LAM, COL_I, COL_{IV} and FIB) patterned onto PIPAAm were imaged using optical phase microscopy, allowing analysis of planar dimensions and verification of pattern

fidelity. The nanoFabric release from the PIPAAm was analyzed using digital video microscopy. Experiments were performed in a custom, heated stage on an inverted microscope with phase-objectives coupled to a Sony DCS-V3 digital camera capable of video (640x480 pixels, 25 fps) or still (3072x2304 pixels) imaging modes. Cover slips with the protein nanoFabrics adhered to the PIPAAm were placed in phosphate buffered saline solution or deionized water at 37°C and observed as the temperature was decreased to 32°C, causing the PIPAAm to dissolve (hydrophobic to hydrophilic transition) and release the nanoFabric. Video and image files were loaded into ImageJ (National Institutes of Health)[36] for morphometric analysis of nanoFabric dimensional changes.

3. Analysis of protein nanoFabric ultrastructure

High-resolution images of platinum-coated FN nanoFabrics pre- and post-release from the PIPAAm films were obtained using scanning electron microscopy (Zeiss Supra 55 VP, field emission) and analyzed using ImageJ software. Analysis of sub-micrometer structures, including the nodular domains in the relaxed FN nanoFabrics, was performed using custom MATLAB code (MathWorks, Inc.). Briefly, SEM images were normalized, and the nodules were counted. The diameter of the nodules was quantified using binary, watershed and morphometric image processing techniques.

The FN nanoFabric thickness was quantified using atomic force microscopy (AFM, MFP-3D, Asylum Research) in both the dry state adhered to PIPAAm and in the hydrated state adhered to a PDMS surface. The nanoFabrics adhered to PIPAAm were kept dry to prevent release and were scanned in air using tapping mode AFM. NanoFabrics were released directly onto PDMS substrates by making conformal contact during the thermal transition, allowing structural investigation of the nanoFabric after fibrillogenesis. The nanoFabrics adhered to PDMS were scanned in phosphate buffered saline using contact mode AFM. NanoFabrics scanned post-release were dried to a glass cover slip and imaged using AC mode in air (Cypher, Asylum Research). Topographic images were used to quantify nanoFabric thickness and lateral dimensions in the wet and dry states using the IGOR Pro software environment (WaveMetrics, Inc.).

Immunofluorescent staining was used to visualize nanoFabrics and verify constituent proteins in multi-component structures. Reagents were obtained from Sigma unless otherwise indicated. The FN was stained with a mouse anti-FN monoclonal primary antibody followed by a goat anti-mouse rhodamine conjugated secondary. The LAM was stained with a rabbit anti-LAM polyclonal primary antibody followed by a goat anti-rabbit Alexa Flour 488 conjugated secondary (Invitrogen). Samples were imaged using an inverted light microscope (Model DMI 6000B, Leica) in epifluorescense with a Coolsnap HQ digital camera (Roper Scientific). The COL_I-FITC conjugate nanoFabrics were viewed directly using a laser scanning confocal microscope (Model LSM 5 Live Zeiss). Image post-processing was performed with ImageJ software to enhance contrast-brightness, merge color channels and insert scale bars.

4. Stretching nanoFabrics with surface tension

Protein nanoFabrics were stretched to determine the extensibility. Fabrication of a 20x20 FN line nanoFabric serially patterned at 90º was used in order to have orthogonally patterned fibrils with the goal of seeing differential stretching in the same nanoFabric. Stretching of the ~8 nm thick nanoFabric (50 µg/mL) was achieved using the surface tension of evaporating water droplets on a glass cover slip (Movie S5).[5] Briefly, nanoFabrics were released from PIPAAm in 10 mL of DI water and then the water was removed leaving a thin film of water on the cover slip covering the nanoFabric. As the water film began to evaporate it broke apart forming water droplets partly covering regions of the nanoFabric. The nanoFabric would become trapped at the air/water interface of the droplet and would be pulled (stretched) normal to the receding water/glass contact line. As the nanoFabric was de-wetted it adhered

to the glass cover slip preserving its stretched or relaxed state. Once the water completely evaporated, samples were either imaged directly in air by AFM or coated with platinum and imaged by SEM.

5. Reversible stretching of fibronectin nanoFabrics

Protein nanoFabrics were reversibly stretched to quantify the extensibility. A micromanipulator was used as schematically illustrated in Supporting Figure S4a and S4b. NanoFabrics were patterned onto PIPAAm coated cover slips as previously described, after which drops of PDMS prepolymer were deposited and cured on top. The PDMS drops served as supports to which the nanoFabrics adhered. The tip of of the micromanipulator was similarly coated with PDMS to serve as a hydrophobic handle by which to grab the nanoFabrics. For these experiments the nanoFabrics were released and stretched in DI water. The applied strain was either measured by tracking the displacement of the micromanipulator relative to the anchor point of the nanoFabric (Figs. S4, S5 and S6) or by tracking displacement of particulates attached to the nanoFabrics (Fig. S4).

6. Formation of engineered cardiac tissue with fibronectin nanoFabrics

Neonatal rat ventricular cardiomyocytes were isolated from 2-day old neonatal Sprague-Dawley using previously described methods.[21] All procedures were approved by the Harvard Animal Care and Use Committee. Reagents were obtained from Sigma unless otherwise indicated. Ventricles were surgically isolated and homogenized by washing in Hanks balanced salt solution followed by digestion with trypsin and collagenase with agitation overnight at 4°C. Subsequently, cells were re-suspended in M199 culture medium supplemented with 10% (v/v) heat-inactivated fetal bovine serum (FBS), 10 mM HEPES, 3.5 g/L glucose, 2mM L-glutamine, 2 mg/L vitamin B-12, and 50 U/mL penicillin and seeded at a density of 350,000 cells/mL. Samples were incubated under standard conditions at 37°C and 5% CO_2. After an additional 48 hours the media was exchanged with maintenance media (M199 media supplemented as above but with 2% FBS) to minimize growth of fibroblasts inevitably present in the primary harvest cardiomyocyte population. Subsequently, media was exchanged with maintenance media every 48 hours until use, typically 3 to 5 days.

Cardiomyocytes were seeded onto FN nanoFabrics either before or after release from the PIPAAm coated cover slips. For seeding pre-release, cover slips were placed in 6-well plates, pre-heated to 37ºC and seeded with the cell suspension. Maintaining temperature above 35ºC ensured that the nanoFabric did not prematurely release from the PIPAAm. For seeding post-release, nanoFabrics were transferred from the PIPAAm coated cover slip to a PDMS frame designed to support overall nanoFabric shape and planar dimensions during cell seeding. PDMS frames were ~2 mm thick and were adhered to the nanoFabric before dissolution of the PIPAAm. As the PIPAAm dissolved, the nanoFabric adhered to the PDMS frame.

For immunofluorescent staining, FN nanoFabrics were released on to PDMS substrates and cardiomyocytes were then seeded. After 3 days cardiomyocytes were fixed in 4% paraformaldhyde and then stained for F-actin using phalloidin conjugated to Alexa Fluor 488 and FN using mouse anti-FN primary antibody and goat anti-mouse secondary antibody conjugated to rhodamine. Fluorescent images were obtained using a Zeiss LSM 5 Live confocal microscope and post-processed using ImageJ image processing software.

7. Functional assessment of engineered cardiac tissue

Experiments on engineered cardiac tissue were conducted at 37°C in M199 media (2% FBS) or in normal Tyrode's solution[21] at room temperature (~22°C). Video microscopy was conducted using an inverted microscope with phase-objectives coupled to a Sony DCS-V3 digital camera capable of video (640x480 pixels, 25 fps) or still (3072x2304 pixels) imaging modes. Analysis of contractility was performed in a post-processing step by tracking the frame-to-frame displacement with image processing

software. Video clips were converted from MPEG to uncompressed AVI and opened in ImageJ as image stacks. The displacement of the cardiac muscle during contraction was tracked manually by choosing a reference point on the tissue or cell and using the ImageJ *Manual Tracking* plug-in to record the position in each frame.

SUPPORTING FIGURES

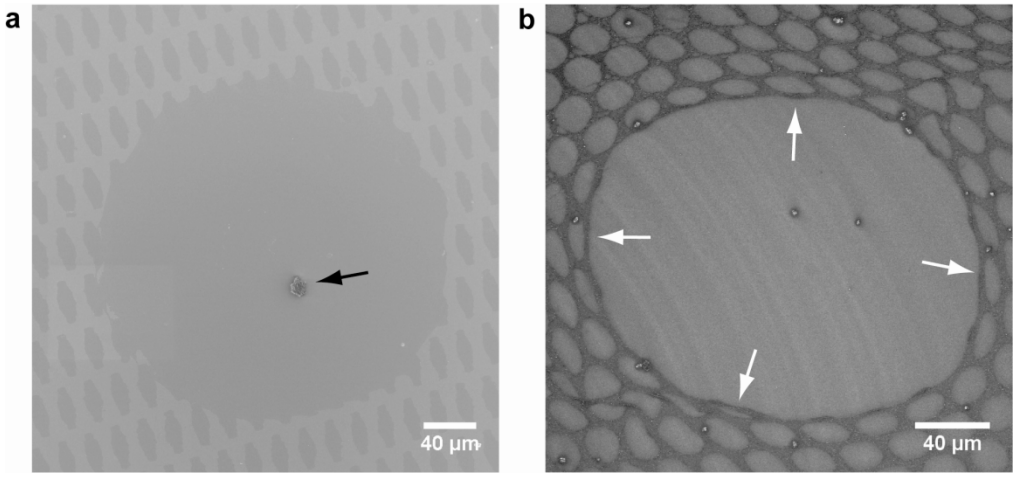

Figure S1. Example of the defects that occur in the protein nanoFabrics as a result of the microcontact printing process. (a) A net-like pattern of FN was deposited onto PIPAAm and imaged by SEM. A dust particle (black arrow) prevented conformal contact between the PDMS stamp and the PIPAAm leaving and air bubble that prevented FN transfer. (b) A FN nanoFabric with a similar net-like pattern imaged by SEM after thermal release from the PIPAAm. The hole in the nanoFabric is the results of a patterning defect due to dust similar to that shown in (a). The FN nanoFabric can support these small defects without failing, but there is deformation of the nanoFabric around the hole (white arrows), indicating that the defect creates a stress concentration. NanoFabric defects due to dust particles can be prevented by fabrication in a cleanroom.

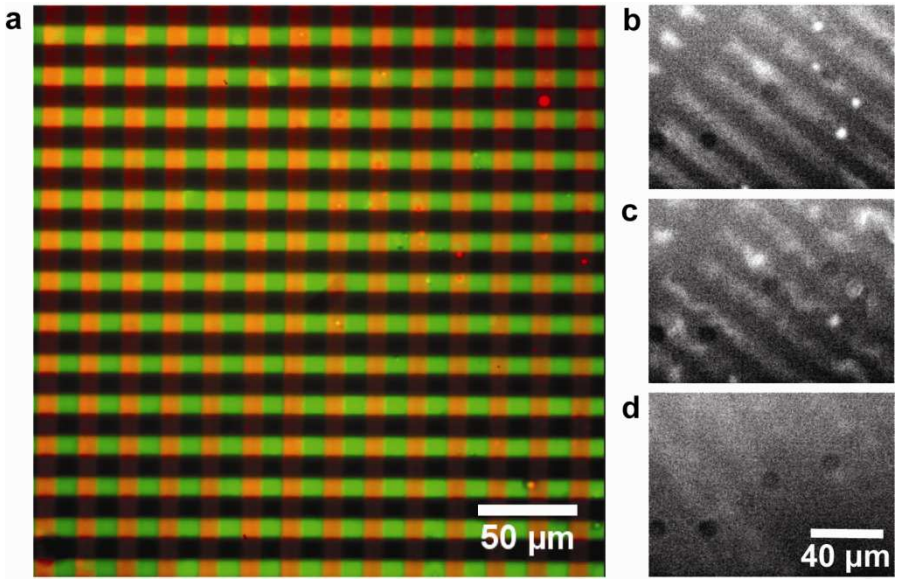

Figure S2. Example of the inability of polysaccharides (dextran) patterned onto PIPAAm to form integrated nanoFabrics (i.e., fibrillogenesis does not occur). (a) Example of 10x10 lines of 500kDa dextran-FITC (green, horizontal lines) and then 70 kDa dextran-TRITC (red, vertical lines) serially microcontact printed onto PIPAAm at an angle 90º. This confirms that the dextran is deposited on the PIPAAm with high-fidelity, similar to the LAM and FN protein nanoFabric (Fig. 1g). (b, c and d) 10x10 lines of 70 kDa dextran-TRITC patterned onto PIPAAm in (b) became distorted as the PIPAAm was thermally triggered to dissolve in (c) and dissolved into solution along with PIPAAm in (d).

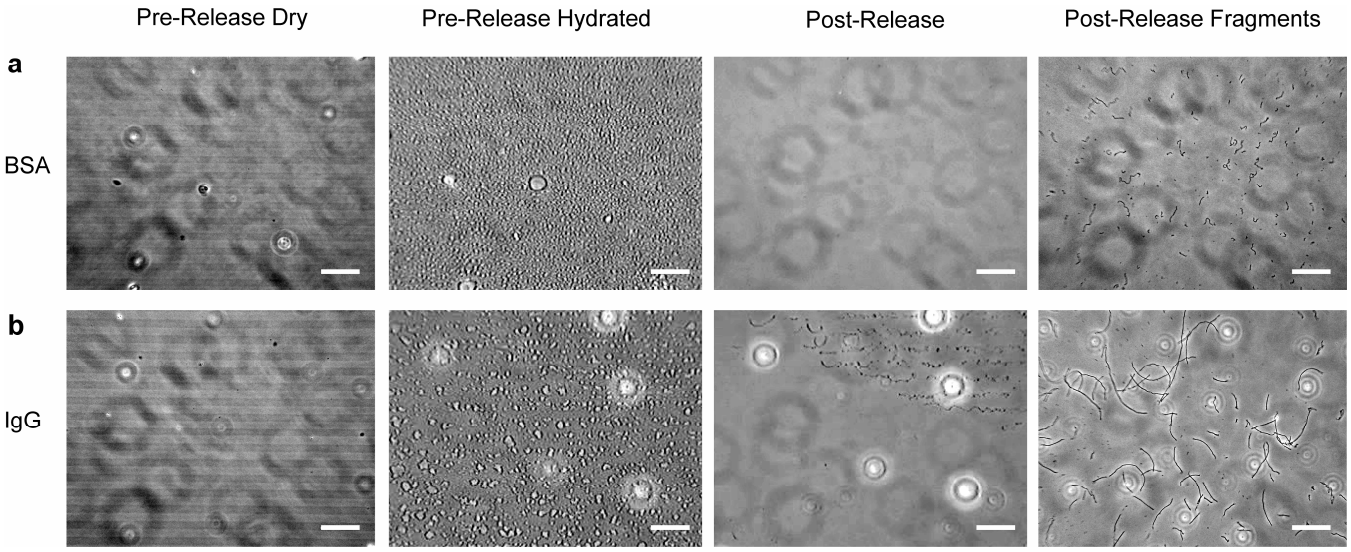

Figure S3. Patterning and release of bovine serum albumin (BSA) and immunoglobulin G (IgG) on PIPAAm as a control experiment. (a) BSA incubated on the PDMS stamp at 1 mg/mL formed patterned lines on PIPAAm, but mostly dissolved upon thermal release. There were some small fragments of BSA that were produced, typically less than 10 μm in length. (b) IgG incubated on the PDMS stamp at 50 μg/mL formed patterned lines on the PIPAAm, and either dissolved or formed short fibrils upon thermal release. The IgG fibrils were of various lengths, but were typically 10 to 30 μm long. IgG fibrils never formed long nanoFabrics 100's of micrometers to centimeters long as observed with the ECM protein-based nanoFabrics. Scale bars are 50 μm.

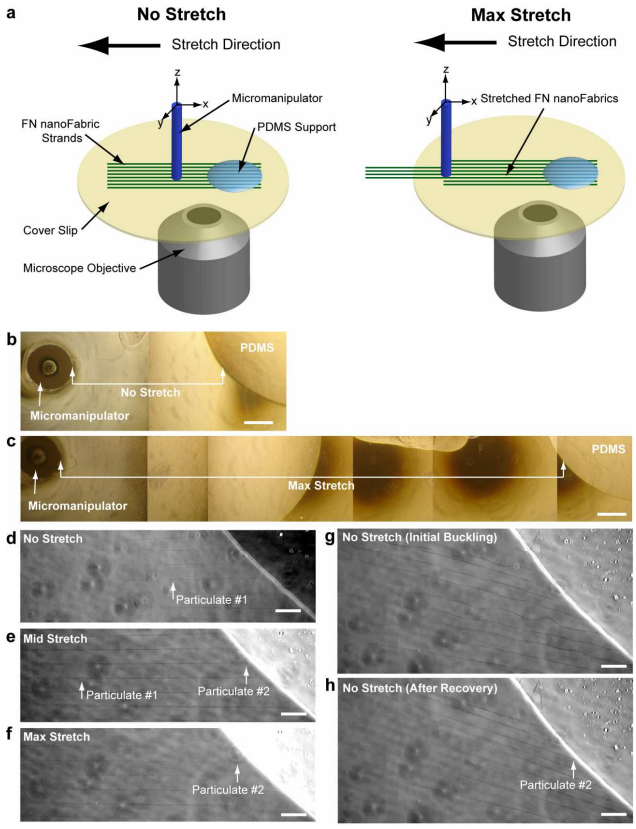

Figure S4. FN nanoFabric strands 10 μm wide and >1 mm long (pre-release) were uniaxially, reversibly stretched between a PDMS support onto which they were released and a micromanipulator that was attached to the free ends. (a) Schematic of the experimental setup for stretching the nanoFabrics. FN nanoFabric strands were adhered to a cover slip using PDMS as the 'glue' and then a PDMS coated micromanipulator probe was used to grab the free ends of the nanoFabrics and stretch them uniaxially. This was done in a Petri dish filled with DI water and observed using optical phase microscopy. (b) A low magnification image created by stitching together multiple fields of view shows the relative position of the PDMS support and the micromanipulator probe when starting the uniaxial stretch. (c) A similar image at maximum stretch indicates a total stretch ratio of 3.85 has been applied. (d) Optical phase imaging of 7 parallel FN nanoFabric strands bound on the right side to a PDMS support and uniaxially stretched to the left using a micromanipulator. The white arrows indicate particulates used as a fiduciary mark to track the applied strain. (e) Particulate #1 has moved to the left and indicates the nanoFabric has undergone 1.94-fold stretch. As stretch is continued particulate #1 moves out of view so particulate #2 on an adjacent strand is tracked. (f) At maximum stretch tracking particulate #2 indicates the nanoFabric has undergone an additional 2.27-fold stretch, for a total 1-D stretch ratio of 4.39 and a Lagrange strain of 912%. Note that no nanoFabrics failed during this stretch, which represents the total travel range of our micromanipulator system. (g) FN nanoFabrics contract back to the original length after releasing the applied stretch. Note that rapid decrease in strain causes an initial buckling morphology of the nanoFabric strands, but this rapidly dissipates (see Supporting Movie 6). (g) Tracking particulate #2 identified in (e) indicates that the nanoFabric reversibly contracts back to its original length when the applied strain is removed. NanoFabrics did not fail during this experiment, repeated three times to demonstrate reversibility. Scale bars are 500 μm in (b) and (c) and 10 μm in (d) through (h).

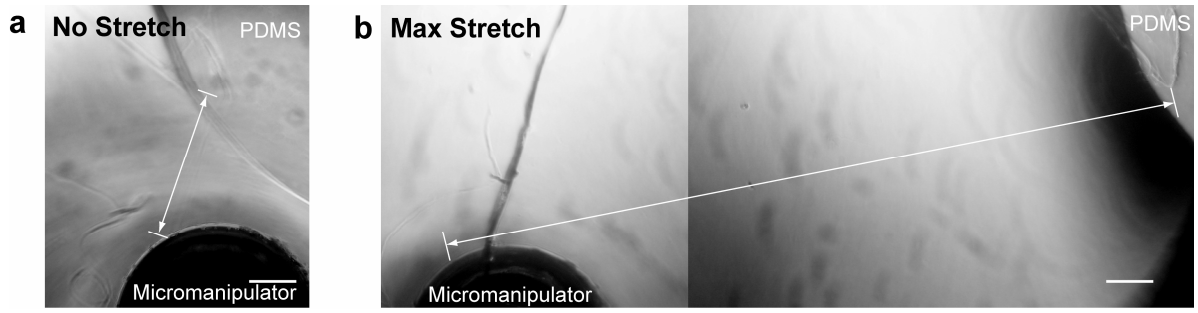

Figure S5. FN nanoFabric strands were stretched ~6 fold. (a) Optical image showing the position of the micromanipulator and PDMS support between which a FN nanoFabric strand is attached. (b) The micromanipulator was moved to the left until the nanoFabric failed, demonstrating a stretch ratio of 5.92 between the no stretch and maximum stretch positions, a 1-dimensional Lagrange strain of ~1,700%. It was not possible to determine definitively if the nanoFabric itself failed or if the adhesion between the nanoFabric and the PDMS-coated micromanipulator tip failed.

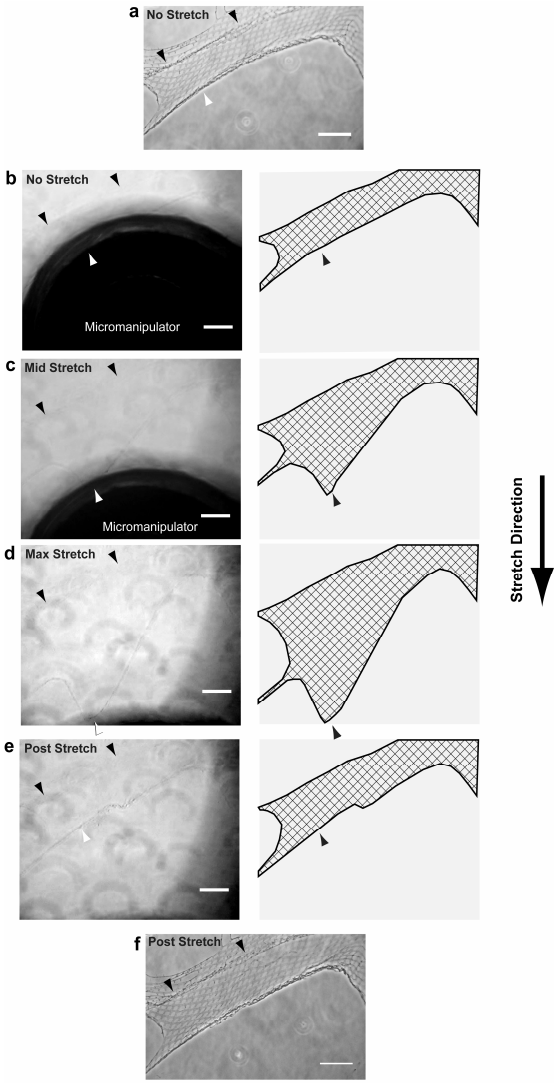

Figure S6. A 2-D FN nanoFabric was reversibly stretched ~3-fold. (a) Optical image (pre-stretch) of a 2-D FN nanoFabric composed of orthogonal, 20x20 FN strands producing a square lattice architecture. The region of the nanoFabric between the black arrowheads and the white arrowhead is not attached to the underlying cover slip and can be stretched. (b) A micromanipulator with a PDMS-coated tip is lowered onto the nanoFabric and adheres to the lower edge as indicated by the white arrowhead. Note that the micromanipulator interferes with the phase contrast imaging, making it difficult to view the interior of the nanoFabric, though the edges can be discerned. The graphic to the right is a schematic of the border of the 2-D nanoFabric to show deformation as it is stretched, the black arrowhead shows where the micromanipulator is attached. Please see Supporting Movie S7 for a clearer image illustrating the stretch experiment. (c) The micromanipulator is moved down (-Y direction) and stretches the nanoFabric, as observed during mid stretch. (d) Near maximum stretch the micromanipulator has moved to the bottom of the field of view and the nanoFabric has been stretched ~3.1 fold when comparing the relative positions of the black and white arrowheads in (b) to (d). (e) The adhesion of the nanoFabric to the micromanipulator fails and the 2-D fabric rapidly contracts and regains its original shape. (f) Comparison of the post stretch to pre stretch (a) nanoFabric shows that the deformation was elastic and reversible. See Supporting Movie S7 for additional information. Scale bars are 100 μm.

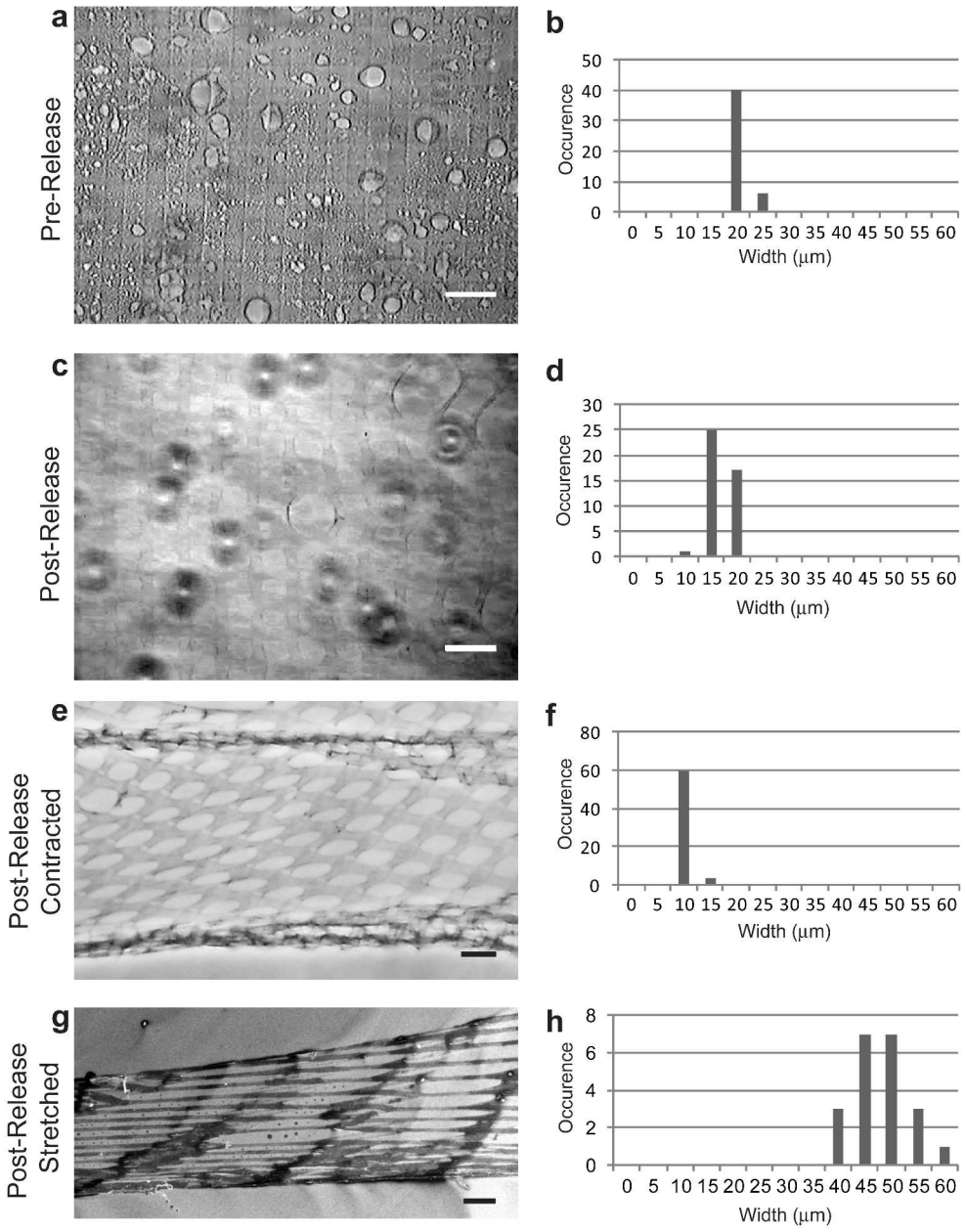

Figure S7. Analysis of stretch and contraction of FN strands within a 2-D nanoFabric. (a) FN 20x20 nanoFabric lines were orthogonally patterned to create a square lattice architecture. Pre-release the FN lines are 19 ± 1 μm wide as shown in the corresponding histogram, confirming that FN is transferred from the PDMS stamp to the PIPAAm at the intended dimensions. (b) The post-release nanoFabric maintains the same approximate pitch, but the pre-stress in the nanoFabric causes the strands' width to contract slightly to 14 ± 2 μm. (c) Allowing the nanoFabric to contract in overall XY dimensions results in a similar decrease in the strand's width, in this case to 8 ± 1 μm. (d) Stretching the nanoFabric (this is the same nanoFabric from Fig. 5c) along one axis causes the FN strands orthogonally oriented to increase in width to 46 ± 5 μm. The differences in the median values between these conditions are greater than would be expected by chance; there is a statistically significant difference in FN strand width (P = <0.001) using a Kruskal-Wallis One Way Analysis of Variance on Ranks. Scale bars are 50 μm in (a), (b) and (c), and 25 μm in (d).

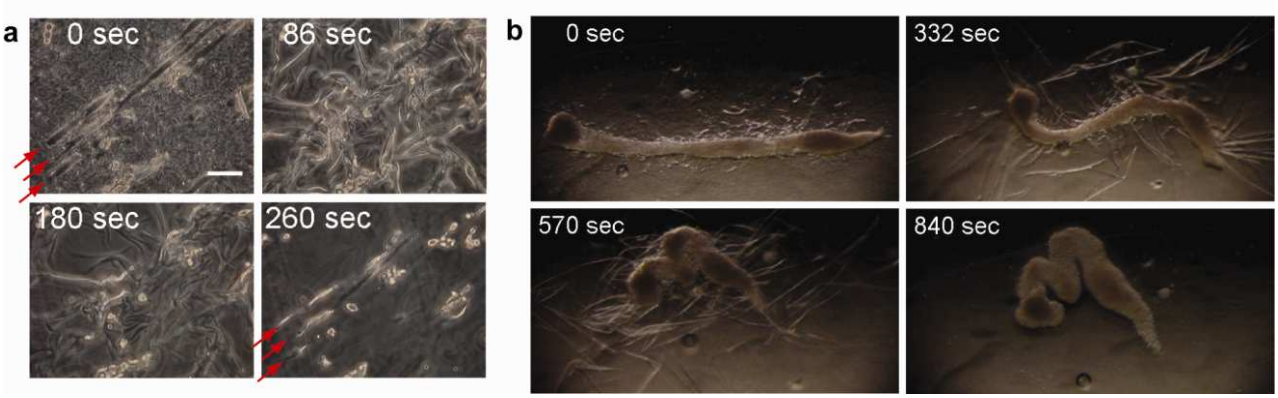

Figure S8. Tissue engineered myocardium formed by seeding cardiomyocytes on FN nanoFabrics prior to thermal release. (a) Seeding cardiomyocytes on FN nanoFabrics prior to release at low-density produced cell "threads" when the PIPAAm was thermally triggered to dissolve. Red arrows indentify three strands of myocardium before (0 sec) and after (260 sec) thermal release. (b) Larger myocardial tissues were engineered by seeding cardiomyocytes at high-density so continuous tissue was formed and then released as a free-standing muscle construct. The spiral-like curvature of the muscle tissue spontaneously manifested.

SUPPORTING MOVIES

Movie S1. Thermal release of FN nanoFabric lines (~8 nm thick)
The thermal release of FN nanoFabric from PIPAAm in DI water. The nanoFabric consists of 20 μm wide, 20 μm spaced FN lines stamped at a concentration of 50 μg/mL (~8 nm thick by AFM). Thermal release occurs as the PIPAAm hydrates and dissolves at <35ºC.

Movie S2. Thermal release of FN nanoFabric lines (~2 nm thick)
The thermal release of FN nanoFabric from PIPAAm in DI water. The nanoFabric consists of 20 μm wide, 20 μm spaced FN lines stamped at a concentration of 2.5 μg/mL (~2 nm thick by AFM). Thermal release occurs as the PIPAAm hydrates and dissolves at <35ºC.

Movie S3. Thermal release of FN nanoFabric 'net'
The thermal release of a multi-layered FN nanoFabric from PIPAAm in DI water. The nanoFabric consists of 15 μm wide, 15 μm spaced horizontal FN lines and 15 μm wide, 15 μm spaced vertical FN lines stamped at a concentration of 50 μg/mL. Thermal release occurs as the PIPAAm hydrates and dissolves at ~35ºC. Some of the horizontal lines of the nanoFabric can be observed to break during release as the unsupported structure undergoes stress relaxation.

Movie S4. Thermal release of micropatterned dextran on PIPAAm
The thermal release of 10x10 lines of 70 kDa dextran-TRITC patterned onto PIPAAm. Thermal release occurs as the PIPAAm hydrates and dissolves at ~35ºC. A nanoFabric does not form, as the dextran dissolves back into the buffer along with the PIPAAm.

Movie S5. Stretching of nanoFabrics be de-wetting of water droplets
The nanoFabrics were stretched by the surface tension of evaporating, de-ionized water droplets as they de-wet the protein onto glass. Orthogonally patterned 20x20 FN lines form a net-like pattern, the linear FN strands are at the edge of the pattern and can be seen moving during the de-wetting process.

Movie S6. Reversible stretching of linear FN nanoFabric strands.
FN 10x10 nanoFabric strands were reversibly stretched with a micromanipulator as illustrated in Supporting Figure S4. The applied strain was measured at the microscale by tracking the displacement of particulates attached to the nanoFabrics. Using the total displacement range of the micromanipulator resulted in a 4.3-fold extension corresponding to 1-D Lagrange strain of %. The nanoFabrics responded elastically when the strain was removed by revesible contracting back to the original length. Interestingly, upon removal of strain the nanoFabric strands could be seen to briefly buckle, perhaps indicating the dissipation of internal stress.

Movie S7. Reversible stretching of 2-D FN nanoFabric.
FN 20x20 nanoFabric strands were orthogonally patterned to form a 2-D square lattice architecture. Stretching the nanoFabric with a micromanipulator demonstrates ~3 fold reversible stretching. Video speed is 2X real time.

Movie S8. FN nanoFabrics support mechanical loading by cardiomyocytes when tissue engineered into a papillary-like muscle
A tissue engineered papillary muscle-like strand of myocardium. A single strand FN nanoFabric ~20 μm wide and 2 mm long was supported at the ends by adhering to a PDMS support. Cardiomyocytes

were subsequently seeded onto the nanoFabric and formed a muscle strand after 3 days in culture and contracted spontaneously.

Movie S9. Release of engineered myocardium
Tissue engineered myocardium generated on FN nanoFabrics and then released from the PIPAAm substrate into solution.

Movie S10. Release of cardiomyocyte "threads"
Strands of myocardium ~20 μm wide grown on FN nanoFabrics and then released from the PIPAAm substrate into as free-floating muscle strands.

SUPPORTING REFERENCES

1. Kadler, K. E.; Hill, A.; Canty-Laird, E. G. *Current Opinion in Cell Biology* **2008,** 20, (5), 495-501.
2. Mao, Y.; Schwarzbauer, J. E. *Matrix Biology* **2005,** 24, (6), 389-399.
3. Leiss, M.; Beckmann, K.; Girós, A.; Costell, M.; Fässler, R. *Current Opinion in Cell Biology* **2008,** 20, (5), 502-507.
4. Little, W. C.; Smith, M. L.; Ebneter, U.; Vogel, V. *Matrix Biology* **2008,** 27, (5), 451-461.
5. Ulmer, J.; Geiger, B.; Spatz, J. P. *Soft Matter* **2008,** 4, (10), 1998-2007.
6. Ahmed, Z.; Underwood, S.; Brown, R. A. *Tissue Engineering* **2003,** 9, (2), 219-231.
7. Barber, T. A.; Mathis, T.; Ihlenfeld, J. V.; Cooper, S. L.; Mosher, D. F. *Scanning Electron Microscopy* **1978**, (2), 431-440.
8. Chen, Y.; Wu, Y.; Cai, J. *Biochemical and Biophysical Research Communications* **2007,** 361, (2), 391-397.
9. Hull, J. R.; Tamura, G. S.; Castner, D. G. *Biophys. J.* **2007,** 93, (8), 2852-2860.
10. Bergkvist, M.; Carlsson, J.; Oscarsson, S. *Journal of Biomedical Materials Research* **2003,** 64A, (2), 349-356.
11. Schwarzbauer, J. E.; Sechler, J. L. *Current Opinion in Cell Biology* **1999,** 11, (5), 622-627.
12. Antia, M.; Baneyx, G.; Kubow, K. E.; Vogel, V. *Faraday Discussions* **2008,** 139, 229-249.
13. Antia, M.; Islas, L. D.; Boness, D. A.; Baneyx, G.; Vogel, V. *Biomaterials* **2006,** 27, (5), 679-690.
14. Baugh, L.; Vogel, V. *Journal of Biomedical Materials Research: Part A* **2004,** 69A, (3), 525-534.
15. Baneyx, G.; Baugh, L.; Vogel, V. *Proceedings of the National Academy of Sciences of the United States of America* **2002,** 99, (8), 5139-5143.
16. Smith, M. L.; Gourdon, D.; Little, W. C.; Kubow, K. E.; Eguiluz, R. A.; Luna-Morris, S.; Vogel, V. *PLoS Biology* **2007,** 5, (10), e268.
17. Wierzbicka-Patynowski, I.; Schwarzbauer, J. E. *J Cell Sci* **2003,** 116, (16), 3269-3276.
18. Sechler, J. L.; Rao, H.; Cumiskey, A. M.; Vega-Colon, I.; Smith, M. S.; Murata, T.; Schwarzbauer, J. E. *J. Cell Biol.* **2001,** 154, (5), 1081-1088.
19. Whitesides, G. M.; Ostuni, E.; Takayama, S.; Jiang, X. Y.; Ingber, D. E. *Annual Review Of Biomedical Engineering* **2001,** 3, 335-373.
20. Khademhosseini, A.; Langer, R.; Borenstein, J.; Vacanti, J. P. *Proceedings Of The National Academy Of Sciences Of The United States Of America* **2006,** 103, (8), 2480-2487.
21. Feinberg, A. W.; Feigel, A.; Shevkoplyas, S. S.; Sheehy, S.; Whitesides, G. M.; Parker, K. K. *Science* **2007,** 317, (5843), 1366-1370.
22. Feinberg, A. W.; Wilkerson, W.; Seegert, C.; Gibson, A. L.; Wilson, L. H.; Brennan, A. B. *Journal of Biomedical Materials Research Part A* **2007,** 86A, (2), 522-534.
23. Chen, C. S.; Mrksich, M.; Huang, S.; Whitesides, G. M.; Ingber, D. E. *Science* **1997,** 276, (5317), 1425-8.
24. Hatakeyama, H.; Kikuchi, A.; Yamato, M.; Okano, T. *Biomaterials* **2007,** 28, (25), 3632-3643.
25. Miyahara, Y.; Nagaya, N.; Kataoka, M.; Yanagawa, B.; Tanaka, K.; Hao, H.; Ishino, K.; Ishida, H.; Shimizu, T.; Kangawa, K.; Sano, S.; Okano, T.; Kitamura, S.; Mori, H. *Nature Medicine* **2006,** 12, (4), 459-465.
26. Akiyama, Y.; Kikuchi, A.; Yamato, M.; Okano, T. *Langmuir* **2004,** 20, (13), 5506-5511.
27. Kushida, A.; Yamato, M.; Konno, C.; Kikuchi, A.; Sakurai, Y.; Okano, T. *Journal Of Biomedical Materials Research* **1999,** 45, (4), 355-362.

28. Canavan, H. E.; Cheng, X.; Graham, D. J.; Ratner, B. D.; Castner, D. G. *Langmuir* **2005,** 21, (5), 1949-1955.
29. Williams, C.; Tsuda, Y.; Isenberg, B. C.; Yamato, M.; Shimizu, T.; Okano, T.; Wong, J. Y. *Advanced Materials* **2008,** 21, (21), 2161-2164.
30. Wadajkar, A.; Koppolu, B.; Rahimi, M.; Nguyen, K. *Journal of Nanoparticle Research* **2009,** 11, (6), 1375-1382.
31. Sotomayor, M.; Schulten, K. *Science* **2007,** 316, (5828), 1144-1148.
32. Rief, M.; Gautel, M.; Oesterhelt, F.; Fernandez, J. M.; Gaub, H. E. *Science* **1997,** 276, (5315), 1109-1112.
33. Oberhauser, A. F.; Badilla-Fernandez, C.; Carrion-Vazquez, M.; Fernandez, J. M. *Journal of Molecular Biology* **2002,** 319, (2), 433-447.
34. Tan, J. L.; Liu, W.; Nelson, C. M.; Raghavan, S.; Chen, C. S. *Tissue Engineering* **2004,** 10, (5-6), 865-872.
35. Toworfe, G. K.; Composto, R. J.; Adams, C. S.; Shapiro, I. M.; Ducheyne, P. *Journal Of Biomedical Materials Research Part A* **2004,** 71A, (3), 449-461.
36. Rasband, W. S. *ImageJ*, U. S. National Institutes of Health: Bethesda, Maryland, USA, 1997-2006.